Observation of $D_s^+ \to p\bar{n}$ and confirmation of its large branching fraction

M. Ablikim,[1] M. N. Achasov,[9,d] S. Ahmed,[14] M. Albrecht,[4] M. Alekseev,[55a,55c] A. Amoroso,[55a,55c] F. F. An,[1] Q. An,[52,42] J. Z. Bai,[1] Y. Bai,[41] O. Bakina,[26] R. Baldini Ferroli,[22a] Y. Ban,[34] K. Begzsuren,[24] D. W. Bennett,[21] J. V. Bennett,[5] N. Berger,[25] M. Bertani,[22a] D. Bettoni,[23a] F. Bianchi,[55a,55c] E. Boger,[26,b] I. Boyko,[26] R. A. Briere,[5] H. Cai,[57] X. Cai,[1,42] O. Cakir,[45a] A. Calcaterra,[22a] G. F. Cao,[1,46] S. A. Cetin,[45b] J. Chai,[55c] J. F. Chang,[1,42] G. Chelkov,[26,b,c] G. Chen,[1] H. S. Chen,[1,46] J. C. Chen,[1] M. L. Chen,[1,42] P. L. Chen,[53] S. J. Chen,[32] X. R. Chen,[29] Y. B. Chen,[1,42] W. Cheng,[55c] X. K. Chu,[34] G. Cibinetto,[23a] F. Cossio,[55c] H. L. Dai,[1,42] J. P. Dai,[37,h] A. Dbeyssi,[14] D. Dedovich,[26] Z. Y. Deng,[1] A. Denig,[25] I. Denysenko,[26] M. Destefanis,[55a,55c] F. De Mori,[55a,55c] Y. Ding,[30] C. Dong,[33] J. Dong,[1,42] L. Y. Dong,[1,46] M. Y. Dong,[1,42,46] Z. L. Dou,[32] S. X. Du,[60] P. F. Duan,[1] J. Fang,[1,42] S. S. Fang,[1,46] Y. Fang,[1] R. Farinelli,[23a,23b] L. Fava,[55b,55c] S. Fegan,[25] F. Feldbauer,[4] G. Felici,[22a] C. Q. Feng,[52,42] E. Fioravanti,[23a] M. Fritsch,[4] C. D. Fu,[1] Q. Gao,[1] X. L. Gao,[52,42] Y. Gao,[44] Y. G. Gao,[6] Z. Gao,[52,42] B. Garillon,[25] I. Garzia,[23a] A. Gilman,[49] K. Goetzen,[10] L. Gong,[33] W. X. Gong,[1,42] W. Gradl,[25] M. Greco,[55a,55c] M. H. Gu,[1,42] Y. T. Gu,[12] A. Q. Guo,[1] R. P. Guo,[1,46] Y. P. Guo,[25] A. Guskov,[26] Z. Haddadi,[28] S. Han,[57] X. Q. Hao,[15] F. A. Harris,[47] K. L. He,[1,46] X. Q. He,[51] F. H. Heinsius,[4] T. Held,[4] Y. K. Heng,[1,42,46] T. Holtmann,[4] Z. L. Hou,[1] H. M. Hu,[1,46] J. F. Hu,[37,h] T. Hu,[1,42,46] Y. Hu,[1] G. S. Huang,[52,42] J. S. Huang,[15] X. T. Huang,[36] X. Z. Huang,[32] Z. L. Huang,[30] T. Hussain,[54] W. Ikegami Andersson,[56] M. Irshad,[52,42] Q. Ji,[1] Q. P. Ji,[15] X. B. Ji,[1,46] X. L. Ji,[1,42] X. S. Jiang,[1,42,46] X. Y. Jiang,[33] J. B. Jiao,[36] Z. Jiao,[17] D. P. Jin,[1,42,46] S. Jin,[1,46] Y. Jin,[48] T. Johansson,[56] A. Julin,[49] N. Kalantar-Nayestanaki,[28] X. S. Kang,[33] M. Kavatsyuk,[28] B. C. Ke,[1] T. Khan,[52,42] A. Khoukaz,[50] P. Kiese,[25] R. Kiuchi,[1] R. Kliemt,[10] L. Koch,[27] O. B. Kolcu,[45b,f] B. Kopf,[4] M. Kornicer,[47] M. Kuemmel,[4] M. Kuessner,[4] A. Kupsc,[56] M. Kurth,[1] W. Kühn,[27] J. S. Lange,[27] M. Lara,[21] P. Larin,[14] L. Lavezzi,[55c] H. Leithoff,[25] C. Li,[56] Cheng Li,[52,42] D. M. Li,[60] F. Li,[1,42] F. Y. Li,[34] G. Li,[1] H. B. Li,[1,46] H. J. Li,[1,46] J. C. Li,[1] J. W. Li,[40] Jin Li,[35] K. J. Li,[43] Kang Li,[13] Ke Li,[1] Lei Li,[3] P. L. Li,[52,42] P. R. Li,[46,7] Q. Y. Li,[36] W. D. Li,[1,46] W. G. Li,[1] X. L. Li,[36] X. N. Li,[1,42] X. Q. Li,[33] Z. B. Li,[43] H. Liang,[52,42] Y. F. Liang,[39] Y. T. Liang,[27] G. R. Liao,[11] L. Z. Liao,[1,46] J. Libby,[20] C. X. Lin,[43] D. X. Lin,[14] B. Liu,[37,h] B. J. Liu,[1] C. X. Liu,[1] D. Liu,[52,42] D. Y. Liu,[37,h] F. H. Liu,[38] Fang Liu,[1] Feng Liu,[6] H. B. Liu,[12] H. L. Liu,[41] H. M. Liu,[1,46] Huanhuan Liu,[1] Huihui Liu,[16] J. B. Liu,[52,42] J. Y. Liu,[1,46] K. Liu,[44] K. Y. Liu,[30] Ke Liu,[6] L. D. Liu,[34] Q. Liu,[46] S. B. Liu,[52,42] X. Liu,[29] Y. B. Liu,[33] Z. A. Liu,[1,42,46] Zhiqing Liu,[25] Y. F. Long,[34] X. C. Lou,[1,42,46] H. J. Lu,[17] J. G. Lu,[1,42] Y. Lu,[1] Y. P. Lu,[1,42] C. L. Luo,[31] M. X. Luo,[59] X. L. Luo,[1,42] S. Lusso,[55c] X. R. Lyu,[46] F. C. Ma,[30] H. L. Ma,[1] L. L. Ma,[36] M. M. Ma,[1,46] Q. M. Ma,[1] T. Ma,[1] X. N. Ma,[33] X. Y. Ma,[1,42] Y. M. Ma,[36] F. E. Maas,[14] M. Maggiora,[55a,55c] Q. A. Malik,[54] A. Mangoni,[22b] Y. J. Mao,[34] Z. P. Mao,[1] S. Marcello,[55a,55c] Z. X. Meng,[48] J. G. Messchendorp,[28] G. Mezzadri,[23b] J. Min,[1,42] R. E. Mitchell,[21] X. H. Mo,[1,42,46] Y. J. Mo,[6] C. Morales Morales,[14] N. Yu. Muchnoi,[9,d] H. Muramatsu,[49] A. Mustafa,[4] Y. Nefedov,[26] F. Nerling,[10] I. B. Nikolaev,[9,d] Z. Ning,[1,42] S. Nisar,[8] S. L. Niu,[1,42] X. Y. Niu,[1,46] S. L. Olsen,[35,j] Q. Ouyang,[1,42,46] S. Pacetti,[22b] Y. Pan,[52,42] M. Papenbrock,[56] P. Patteri,[22a] M. Pelizaeus,[4] J. Pellegrino,[55a,55c] H. P. Peng,[52,42] Z. Y. Peng,[12] K. Peters,[10,g] J. Pettersson,[56] J. L. Ping,[31] R. G. Ping,[1,46] A. Pitka,[4] R. Poling,[49] V. Prasad,[52,42] H. R. Qi,[2] M. Qi,[32] T. Y. Qi,[2] S. Qian,[1,42] C. F. Qiao,[46] N. Qin,[57] X. S. Qin,[4] Z. H. Qin,[1,42] J. F. Qiu,[1] K. H. Rashid,[54,i] C. F. Redmer,[25] M. Richter,[4] M. Ripka,[25] A. Rivetti,[55c] M. Rolo,[55c] G. Rong,[1,46] Ch. Rosner,[14] A. Sarantsev,[26,e] M. Savrié,[23b] C. Schnier,[4] K. Schoenning,[56] W. Shan,[18] X. Y. Shan,[52,42] M. Shao,[52,42] C. P. Shen,[2] P. X. Shen,[33] X. Y. Shen,[1,46] H. Y. Sheng,[1] X. Shi,[1,42] J. J. Song,[36] W. M. Song,[36] X. Y. Song,[1] S. Sosio,[55a,55c] C. Sowa,[4] S. Spataro,[55a,55c] G. X. Sun,[1] J. F. Sun,[15] L. Sun,[57] S. S. Sun,[1,46] X. H. Sun,[1] Y. J. Sun,[52,42] Y. K. Sun,[52,42] Y. Z. Sun,[1] Z. J. Sun,[1,42] Z. T. Sun,[21] Y. T. Tan,[52,42] C. J. Tang,[39] G. Y. Tang,[1] X. Tang,[1] I. Tapan,[45c] M. Tiemens,[28] B. Tsednee,[24] I. Uman,[45d] G. S. Varner,[47] B. Wang,[1] B. L. Wang,[46] D. Wang,[34] D. Y. Wang,[34] Dan Wang,[46] K. Wang,[1,42] L. L. Wang,[1] L. S. Wang,[1] M. Wang,[36] Meng Wang,[1,46] P. Wang,[1] P. L. Wang,[1] W. P. Wang,[52,42] X. F. Wang,[44] Y. Wang,[52,42] Y. F. Wang,[1,42,46] Y. Q. Wang,[25] Z. Wang,[1,42] Z. G. Wang,[1,42] Z. Y. Wang,[1] Zongyuan Wang,[1,46] T. Weber,[4] D. H. Wei,[11] P. Weidenkaff,[25] S. P. Wen,[1] U. Wiedner,[4] M. Wolke,[56] L. H. Wu,[1] L. J. Wu,[1,46] Z. Wu,[1,42] L. Xia,[52,42] Y. Xia,[19] D. Xiao,[1] Y. J. Xiao,[1,46] Z. J. Xiao,[31] Y. G. Xie,[1,42] Y. H. Xie,[6] X. A. Xiong,[1,46] Q. L. Xiu,[1,42] G. F. Xu,[1] J. J. Xu,[1,46] L. Xu,[1] Q. J. Xu,[13] Q. N. Xu,[46] X. P. Xu,[40] F. Yan,[53] L. Yan,[55a,55c] W. B. Yan,[52,42] W. C. Yan,[2] Y. H. Yan,[19] H. J. Yang,[37,h] H. X. Yang,[1] L. Yang,[57] Y. H. Yang,[32] Y. X. Yang,[11] Yifan Yang,[1,46] Z. Q. Yang,[19] M. Ye,[1,42] M. H. Ye,[7] J. H. Yin,[1] Z. Y. You,[43] B. X. Yu,[1,42,46] C. X. Yu,[33] J. S. Yu,[29] J. S. Yu,[19] C. Z. Yuan,[1,46] Y. Yuan,[1] A. Yuncu,[45b,a] A. A. Zafar,[54] Y. Zeng,[19] Z. Zeng,[52,42] B. X. Zhang,[1] B. Y. Zhang,[1,42] C. C. Zhang,[1] D. H. Zhang,[1] H. H. Zhang,[43] H. Y. Zhang,[1,42] J. Zhang,[1,46] J. L. Zhang,[58] J. Q. Zhang,[4] J. W. Zhang,[1,42,46] J. Y. Zhang,[1] J. Z. Zhang,[1,46] K. Zhang,[1,46] L. Zhang,[44] T. J. Zhang,[37,h] X. Y. Zhang,[36] Y. Zhang,[52,42] Y. H. Zhang,[1,42] Y. T. Zhang,[52,42] Yang Zhang,[1] Yao Zhang,[1] Yu Zhang,[46] Z. H. Zhang,[6] Z. P. Zhang,[52] Z. Y. Zhang,[57] G. Zhao,[1] J. W. Zhao,[1,42] J. Y. Zhao,[1,46] J. Z. Zhao,[1,42] Lei Zhao,[52,42] Ling Zhao,[1] M. G. Zhao,[33] Q. Zhao,[1] S. J. Zhao,[60] T. C. Zhao,[1] Y. B. Zhao,[1,42] Z. G. Zhao,[52,42] A. Zhemchugov,[26,b] B. Zheng,[53] J. P. Zheng,[1,42] Y. H. Zheng,[46] B. Zhong,[31] L. Zhou,[1,42] Q. Zhou,[1,46] X. Zhou,[57] X. K. Zhou,[52,42] X. R. Zhou,[52,42]

X. Y. Zhou,[1] Xiaoyu Zhou,[19] Xu Zhou,[19] A. N. Zhu,[1,46] J. Zhu,[33] J. Zhu,[43] K. Zhu,[1] K. J. Zhu,[1,42,46] S. Zhu,[1] S. H. Zhu,[51] X. L. Zhu,[44] Y. C. Zhu,[52,42] Y. S. Zhu,[1,46] Z. A. Zhu,[1,46] J. Zhuang,[1,42] B. S. Zou,[1] and J. H. Zou[1]

(BESIII Collaboration)

[1]*Institute of High Energy Physics, Beijing 100049, People's Republic of China*
[2]*Beihang University, Beijing 100191, People's Republic of China*
[3]*Beijing Institute of Petrochemical Technology, Beijing 102617, People's Republic of China*
[4]*Bochum Ruhr-University, D-44780 Bochum, Germany*
[5]*Carnegie Mellon University, Pittsburgh, Pennsylvania 15213, USA*
[6]*Central China Normal University, Wuhan 430079, People's Republic of China*
[7]*China Center of Advanced Science and Technology, Beijing 100190, People's Republic of China*
[8]*COMSATS Institute of Information Technology,*
Lahore, Defence Road, Off Raiwind Road, 54000 Lahore, Pakistan
[9]*G.I. Budker Institute of Nuclear Physics SB RAS (BINP), Novosibirsk 630090, Russia*
[10]*GSI Helmholtzcentre for Heavy Ion Research GmbH, D-64291 Darmstadt, Germany*
[11]*Guangxi Normal University, Guilin 541004, People's Republic of China*
[12]*Guangxi University, Nanning 530004, People's Republic of China*
[13]*Hangzhou Normal University, Hangzhou 310036, People's Republic of China*
[14]*Helmholtz Institute Mainz, Johann-Joachim-Becher-Weg 45, D-55099 Mainz, Germany*
[15]*Henan Normal University, Xinxiang 453007, People's Republic of China*
[16]*Henan University of Science and Technology, Luoyang 471003, People's Republic of China*
[17]*Huangshan College, Huangshan 245000, People's Republic of China*
[18]*Hunan Normal University, Changsha 410081, People's Republic of China*
[19]*Hunan University, Changsha 410082, People's Republic of China*
[20]*Indian Institute of Technology Madras, Chennai 600036, India*
[21]*Indiana University, Bloomington, Indiana 47405, USA*
[22a]*INFN Laboratori Nazionali di Frascati, I-00044 Frascati, Italy*
[22b]*INFN and University of Perugia, I-06100 Perugia, Italy*
[23a]*INFN Sezione di Ferrara, I-44122 Ferrara, Italy;*
[23b]*University of Ferrara, I-44122 Ferrara, Italy*
[24]*Institute of Physics and Technology, Peace Ave. 54B, Ulaanbaatar 13330, Mongolia*
[25]*Johannes Gutenberg University of Mainz, Johann-Joachim-Becher-Weg 45, D-55099 Mainz, Germany*
[26]*Joint Institute for Nuclear Research, Dubna 141980, Moscow region, Russia*
[27]*Justus-Liebig-Universitaet Giessen, II. Physikalisches Institut,*
Heinrich-Buff-Ring 16, D-35392 Giessen, Germany
[28]*KVI-CART, University of Groningen, NL-9747 AA Groningen, The Netherlands*
[29]*Lanzhou University, Lanzhou 730000, People's Republic of China*
[30]*Liaoning University, Shenyang 110036, People's Republic of China*
[31]*Nanjing Normal University, Nanjing 210023, People's Republic of China*
[32]*Nanjing University, Nanjing 210093, People's Republic of China*
[33]*Nankai University, Tianjin 300071, People's Republic of China*
[34]*Peking University, Beijing 100871, People's Republic of China*
[35]*Seoul National University, Seoul 151-747, Korea*
[36]*Shandong University, Jinan 250100, People's Republic of China*
[37]*Shanghai Jiao Tong University, Shanghai 200240, People's Republic of China*
[38]*Shanxi University, Taiyuan 030006, People's Republic of China*
[39]*Sichuan University, Chengdu 610064, People's Republic of China*
[40]*Soochow University, Suzhou 215006, People's Republic of China*
[41]*Southeast University, Nanjing 211100, People's Republic of China*
[42]*State Key Laboratory of Particle Detection and Electronics,*
Beijing 100049, Hefei 230026, People's Republic of China
[43]*Sun Yat-Sen University, Guangzhou 510275, People's Republic of China*
[44]*Tsinghua University, Beijing 100084, People's Republic of China*
[45a]*Ankara University, 06100 Tandogan, Ankara, Turkey*
[45b]*Istanbul Bilgi University, 34060 Eyup, Istanbul, Turkey*
[45c]*Uludag University, 16059 Bursa, Turkey*
[45d]*Near East University, Nicosia, North Cyprus, Mersin 10, Turkey*
[46]*University of Chinese Academy of Sciences, Beijing 100049, People's Republic of China*
[47]*University of Hawaii, Honolulu, Hawaii 96822, USA*

48University of Jinan, Jinan 250022, People's Republic of China
49University of Minnesota, Minneapolis, Minnesota 55455, USA
50University of Muenster, Wilhelm-Klemm-Str. 9, 48149 Muenster, Germany
51University of Science and Technology Liaoning, Anshan 114051, People's Republic of China
52University of Science and Technology of China, Hefei 230026, People's Republic of China
53University of South China, Hengyang 421001, People's Republic of China
54University of the Punjab, Lahore 54590, Pakistan
55aUniversity of Turin, I-10125 Turin, Italy
55bUniversity of Eastern Piedmont, I-15121 Alessandria, Italy
55cINFN, I-10125 Turin, Italy
56Uppsala University, Box 516, SE-75120 Uppsala, Sweden
57Wuhan University, Wuhan 430072, People's Republic of China
58Xinyang Normal University, Xinyang 464000, People's Republic of China
59Zhejiang University, Hangzhou 310027, People's Republic of China
60Zhengzhou University, Zhengzhou 450001, People's Republic of China

The baryonic decay $D_s^+ \to p\bar{n}$ is observed, and the corresponding branching fraction is measured to be $(1.21 \pm 0.10 \pm 0.05) \times 10^{-3}$, where the first uncertainty is statistical and second systematic. The data sample used in this analysis was collected with the BESIII detector operating at the BEPCII e^+e^- double-ring collider with a center-of-mass energy of 4.178 GeV and an integrated luminosity of 3.19 fb^{-1}. The result confirms the previous measurement by the CLEO Collaboration and is of greatly improved precision. This result will improve our understanding of the dynamical enhancement of the W-annihilation topology in the charmed meson decays.

The decay $D_s^+ \to p\bar{n}$ is the only kinematically allowed baryonic decay of the three ground-state charmed mesons D^0, D^+, and D_s^+. It provides a unique probe of hadronic dynamics and is of great importance to the study of weak annihilation decays of charmed mesons [1–5]. At the short-distance level, under the vacuum-insertion approximation,

aAlso at Bogazici University, 34342 Istanbul, Turkey.
bAlso at the Moscow Institute of Physics and Technology, Moscow 141700, Russia.
cAlso at the Functional Electronics Laboratory, Tomsk State University, Tomsk 634050, Russia.
dAlso at the Novosibirsk State University, Novosibirsk 630090, Russia.
eAlso at the NRC "Kurchatov Institute," PNPI, Gatchina 188300, Russia.
fAlso at Istanbul Arel University, 34295 Istanbul, Turkey.
gAlso at Goethe University Frankfurt, 60323 Frankfurt am Main, Germany.
hAlso at Key Laboratory for Particle Physics, Astrophysics and Cosmology, Ministry of Education; Shanghai Key Laboratory for Particle Physics and Cosmology; Institute of Nuclear and Particle Physics, Shanghai 200240, People's Republic of China.
iAlso at Government College Women University, Sialkot 51310 Punjab, Pakistan.
jCurrently at Center for Underground Physics, Institute for Basic Science, Daejeon 34126, Korea.

its branching fraction (BF) is predicted to be very small (of the order 10^{-6}) owing to chiral suppression by the factor $(m_\pi/m_{D_s})^4$ which follows from the partially conserved axial current [4]. This physically corresponds to the mechanism of helicity suppression.

The CLEO Collaboration studied the decay $D_s^+ \to p\bar{n}$ with 13.0 ± 3.6 signal events, resulting in a large BF of $\mathcal{B}(D_s^+ \to p\bar{n}) = (1.30 \pm 0.36^{+0.12}_{-0.16}) \times 10^{-3}$ [6]. This large BF stimulates the interest of theorists. Many phenomenological possibilities have been proposed to explain the apparent discrepancy between theoretical predictions and the experimental measurement, e.g., the not well-justified factorization ansatz due to the light mass of charm quark and the complicated final state interaction at the threshold of $p\bar{n}$ production [2–4], a contribution of additional decay mechanisms such as final state scattering [4], or the effect of the timelike baryonic form factors from the axial vector currents [7]. Experimentally, the confirmation of the observation of the decay $D_s^+ \to p\bar{n}$ by different experiments is highly desirable, and a much improved precision on its decay BF is necessary to distinguish between different phenomenological models and understand the decay dynamics of charmed mesons. The e^+e^- annihilation sample collected at $\sqrt{s} = 4.178$ GeV with the Beijing Spectrometer (BESIII) in 2016, which corresponds to an integrated luminosity of 3.19 fb^{-1} and is roughly 10 times larger in statistics compared to the CLEO data [6], provides a good opportunity for this measurement.

BESIII is a general-purpose detector with 93% coverage of the full solid angle. Details of the detector can be found in Ref. [8]. In 2015, BESIII was upgraded by replacing the two end cap time-of-flight (TOF) systems with a new detectors that use multi-gap resistive plate chambers (MRPC), which achieve a time resolution of 60 ps [9].

A GEANT4-based [10] Monte Carlo (MC) simulation software package, which includes the description of the BESIII detector geometry and its response, is used to generate MC simulated event samples. The simulation includes the beam energy spread and initial state radiation (ISR) in the e^+e^- annihilations modeled with the generator ConExc [11]. The final state radiation from charged tracks is incorporated with the PHOTOS package [12]. The generic MC samples, consisting of the production of open charm processes, the ISR return to low-mass charmonium (ψ) states, and continuum processes (quantum electrodynamics processes and continuum production of light quarks $q\bar{q}$, $q = u$, d, s), have a size corresponding to an integrated luminosity 35 times larger than that of the data. The known particle decays are generated using EVTGEN [13] with the BFs taken from the Particle Data Group (PDG) [14], and the remaining unknown decays of low mass ψ states are generated with LUNDCHARM [15]. We also generate a signal MC sample of 4×10^6 events, which is used to obtain the shapes of kinematic variables in signal decays and to estimate systematic uncertainties. In this analysis, the D_s sample is predominantly produced in the reaction $e^+e^- \to D_s^{*\pm}D_s^{\mp} \to \gamma D_s^+ D_s^-$. For our signal event, the $D_s^{*\pm}D_s^{\mp}$ pair decays to either $D_s^+(\to p\bar{n})D_s^-(\to \text{generic})$ or $D_s^-(\to \bar{p}n)D_s^+(\to \text{generic})$. Throughout the article, charge conjugated modes are implicitly implied, unless otherwise noted.

We fully reconstruct a D_s^- meson, named "single tag (ST)," in eleven decay modes that correspond to 25% of the total decay width [14]: $K_S^0K^-$, $K^-K^+\pi^-$, $K_S^0K^-\pi^0$, $K^-K^+\pi^-\pi^0$, $K_S^0K^+\pi^-\pi^-$, $\pi^-\pi^+\pi^-$, $\pi^-\eta$, $\rho^-\eta$, $\pi^-\eta'$ (with $\eta' \to \pi^+\pi^-\eta$), $\pi^-\eta'$ (with $\eta' \to \gamma\pi^+\pi^-$) and $K^-\pi^+\pi^-$. Then in the ST D_s^- sample, we further require an isolated photon consistent with D_s^{*+} decay and reconstruct the $D_s^+ \to p\bar{n}$ signal in the side recoiling against the D_s^- candidate, referred to as the "double tag (DT)". Both the D_s^+ directly produced in the e^+e^- annihilation and the one from D_s^{*+} decay are considered. Thus, the numbers of ST (N_{ST}^i) and DT (N_{DT}^i) candidates for a specific tag mode i are

$$N_{\text{ST}}^i = 2N_{\text{tot}} \cdot \mathcal{B}_i \cdot \epsilon_{\text{ST}}^i, \qquad (1)$$

$$N_{\text{DT}}^i = 2N_{\text{tot}} \cdot \mathcal{B}_i \cdot \mathcal{B}_{D_s^{*+} \to \gamma D_s^+} \cdot \mathcal{B}_{D_s^+ \to p\bar{n}} \cdot \epsilon_{\text{DT}}^i, \qquad (2)$$

where N_{tot} is the total number of $e^+e^- \to D_s^{*+}D_s^- + \text{c.c.}$ events in the data, $\mathcal{B}_i$, $\mathcal{B}_{D_s^{*+} \to \gamma D_s^+}$, and $\mathcal{B}_{D_s^+ \to p\bar{n}}$ are the BFs for D_s^- tag mode i, $D_s^{*+} \to \gamma D_s^+$, and $D_s^+ \to p\bar{n}$, respectively, and $\epsilon_{\text{ST(DT)}}^i$ is the ST(DT) detection efficiency.

The factor 2 indicates that the signal D_s^+ is either directly produced in the e^+e^- annihilation or from D_s^{*+} decay. Based on Eqs. (1) and (2), combining the eleven ST modes leads to the expression

$$\mathcal{B}_{D_s^+ \to p\bar{n}} = \frac{1}{\mathcal{B}_{D_s^* \to \gamma D_s}} \cdot \frac{N_{\text{DT}}^{\text{tot}}}{\sum_i N_{\text{ST}}^i \cdot \epsilon_{\text{DT}}^i/\epsilon_{\text{ST}}^i}, \qquad (3)$$

where $N_{\text{DT}}^{\text{tot}}$ is the total number of DT signal events reconstructed from all ST modes.

All charged tracks are reconstructed from hits in the main drift chamber (MDC) with a polar angle θ (with respect to the beam direction) within $|\cos\theta| < 0.93$. Charged tracks, except for those from K_S^0 decays, are required to have a point of closest approach to the interaction point (IP) within ± 10 cm along the beam direction and within 1 cm in the plane perpendicular to the beam axis. Particle identification (PID) is performed by combining the specific energy loss dE/dx measured in the MDC and the TOF information. A charged $\pi(K)$ candidate is identified by requiring the PID likelihood value $\mathcal{L}(\pi) > \mathcal{L}(K)$, $\mathcal{L}(\pi) > 0$ ($\mathcal{L}(K) > \mathcal{L}(\pi)$, $\mathcal{L}(K) > 0$).

Photon candidates are reconstructed with energy deposits in the electromagnetic calorimeter (EMC) that are not associated with reconstructed charged tracks. The photon is required to have an energy larger than 25 MeV in the barrel region ($|\cos\theta| < 0.8$), or 50 MeV in the end cap region ($0.86 < |\cos\theta| < 0.92$). To suppress electronic noise and energy deposits unrelated to the events, the shower time in the EMC must be within 700 ns of the event start time [16]. The π^0 and η candidates are reconstructed from $\gamma\gamma$ pairs with an invariant mass $M_{\gamma\gamma}$ within $(0.115, 0.150)$ GeV/c^2 and $(0.50, 0.57)$ GeV/c^2, respectively. Candidates with both photons in the end cap regions are rejected due to the bad energy resolution. To improve the momentum resolution, a 1C kinematic fit is performed, constraining $M_{\gamma\gamma}$ to the nominal π^0 or η mass [14] and requiring $\chi^2 < 30$. The updated momentum of each photon from the kinematic fit is used in the further analysis.

The K_S^0 candidates are reconstructed via the decay $K_S^0 \to \pi^+\pi^-$ by performing a vertex-constrained fit to all oppositely charged track pairs without PID requirements applied. The charged tracks must be within $|\cos\theta| < 0.93$, and have a point of closest approach to the IP within ± 20 cm along the beam direction; no requirement is placed on the point of closest approach in the plane perpendicular to the beam. The χ^2 of the vertex fit must be less than 100. To suppress the combinatorial background, a secondary vertex fit is performed, constraining the direction of the K_S^0 momentum to point back to the IP, and requiring $\chi^2 < 20$. The flight length L, defined as the distance between the common vertex of the $\pi^+\pi^-$ pair and the IP, is obtained in the secondary vertex fit and required to satisfy $L > 2\sigma_L$ for

accepted K_S^0 candidates, where σ_L is the uncertainty of L. The four-momenta after the secondary vertex fit are used in the subsequent analysis. The K_S^0 candidate is required to have a mass within the range $(0.487, 0.511)$ GeV/c^2, corresponding to 3 standard deviations on the mass distribution.

The η' candidates are reconstructed via the prominent decay modes $\eta' \to \pi^+\pi^-\eta$ and $\eta' \to \gamma\pi^+\pi^-$, requiring the invariant masses of $\pi^+\pi^-\eta$ and $\gamma\pi^+\pi^-$ to be within $(0.945, 0.970)$ and $(0.938, 0.978)$ GeV/c^2, respectively. The $\rho^{\pm(0)}$ candidate is selected by requiring the $\pi^\pm\pi^{0(\mp)}$ invariant mass within $(0.6, 0.9)$ GeV/c^2.

In the ST mode $D_s^- \to K^-\pi^+\pi^-$, the $\pi^+\pi^-$ invariant mass is required to be outside the range $(0.480, 0.515)$ GeV/c^2 to avoid double counting with the ST mode $D_s^- \to K_S^0 K^-$.

For a given ST mode, the D_s^- candidates are reconstructed by all possible combinations of selected $K^\pm$, $\pi^\pm$, K_S^0, π^0, η and η' candidates in an event, and are identified with the corresponding invariant mass M_{tag}. To suppress the background from the nonstrangeness excited D^* decay $D^* \to \pi D$, the $\pi^{\pm(0)}$ candidates from D_s^+ decays must have a momentum larger than 100 MeV/c. To further suppress the non-$D_s^{*+}D_s^-$ backgrounds, a variable that represents the invariant mass of the system recoiling against the selected D_s^- candidate is defined as

$$M_{\mathrm{rec}}^2 = \left(E_{\mathrm{cm}} - \sqrt{|\vec{p}_{D_s}|^2 + M_{D_s}^2}\right)^2 - |\vec{p}_{D_s}|^2, \quad (4)$$

where E_{cm} is the center-of-mass energy, $\vec{p}_{D_s}$ is the momentum of the selected D_s^- candidate in the center-of-mass system, and M_{D_s} is the nominal D_s^- mass [14]. In the process $e^+e^- \to D_s^{*+}D_s^- \to D_s^+\gamma D_s^-$, the selected D_s^- candidates are produced either directly in the e^+e^- annihilation or from the decay $D_s^{*-} \to \gamma D_s^-$. The corresponding M_{rec} distribution for the former case peaks at the nominal D_s^{*+} mass $M_{D_s^{*+}}$ [14] smeared by the mass resolution, and that for the latter case has a relatively flat distribution between 2.05 and 2.18 GeV/c^2. The D_s^- candidates are accepted by requiring $2.05 < M_{\mathrm{rec}} < 2.18$ GeV/c^2. The $e^+e^- \to D_s^+D_s^-$ process is highly suppressed by this requirement. For an event with multi-D_s^- candidates for a specific tag mode per charge, only the one with minimum $|M_{\mathrm{rec}} - M_{D_s^{*+}}|$ is kept.

The M_{tag} distributions of the events passing the above selection criteria are shown in Fig. 1 for all ST modes. The ST yields are determined by performing a binned maximum likelihood fit. In the fit, the D_s^- signal is described by the MC-simulated line shape convolved with a Gaussian function representing the resolution difference between data and MC simulation, where the parameters of the Gaussian functions are free parameters the fit. The background is described by Chebychev polynomial functions of the first kind of first or second order. The fit results are superimposed on the data in Fig. 1. For further study, we require that M_{tag} is within 2.5 times the resolution around the D_s^- peak. The requirements on M_{tag}, the ST yields, and the corresponding ST detection efficiencies obtained with
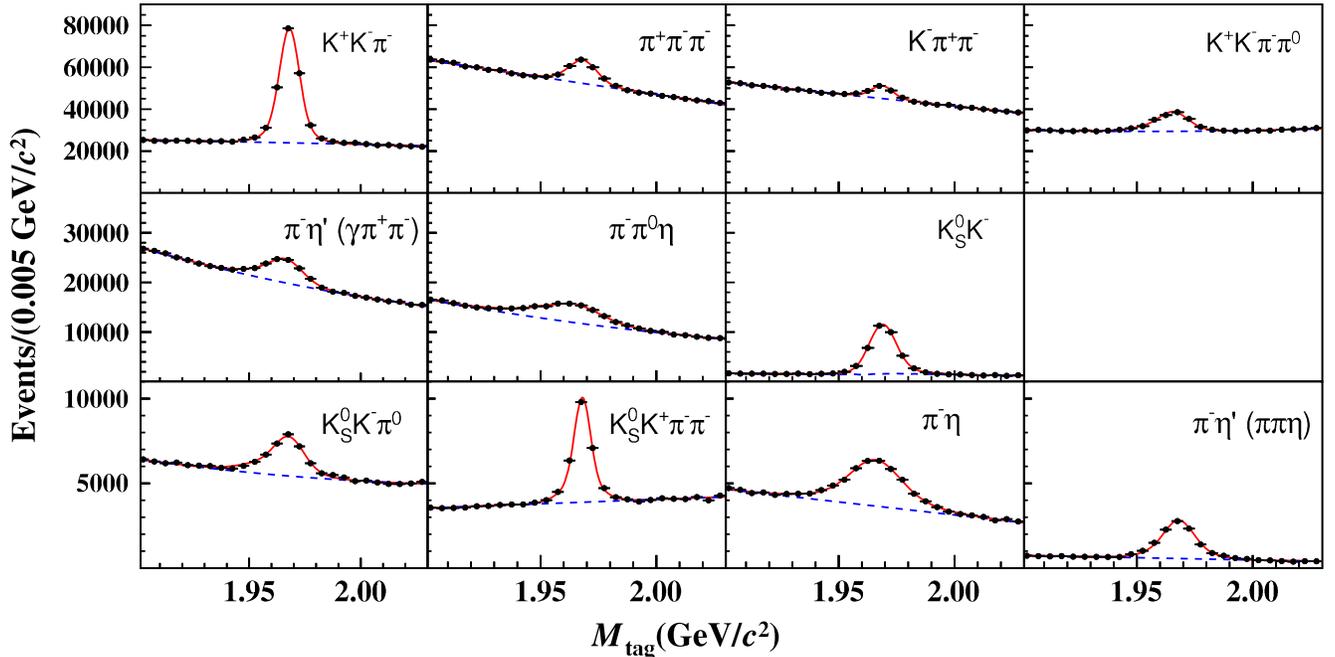

FIG. 1. Fits to the M_{tag} distributions for various ST modes. The dots with error bars show data, the red solid lines are the overall fit results, and the blue dashed curves are the background.

TABLE I.   Requirements on M_{tag}, ST yields, ST and DT detection efficiencies for individual ST modes. The uncertainties are statistical only. The BFs of $\pi^0/\eta \to \gamma\gamma$, $K_S^0 \to \pi^+\pi^-$, $\eta' \to \pi^+\pi^-\eta$ and $\eta' \to \gamma\pi^+\pi^-$ are not included in efficiencies.

ST mode	$M_{\text{tag}}(\text{GeV}/c^2)$	N_{ST}^i	$\epsilon_{\text{ST}}^i(\%)$	$\epsilon_{\text{DT}}^i(\%)$
$K_S^0 K^-$	[1.950,1.990]	30364 ± 231	46.23 ± 0.04	19.12 ± 0.95
$K^+ K^- \pi^-$	[1.950,1.985]	133666 ± 544	39.67 ± 0.02	17.85 ± 0.40
$K_S^0 K^- \pi^0$	[1.930,1.990]	10425 ± 316	15.45 ± 0.03	9.39 ± 0.81
$K^+ K^- \pi^- \pi^0$	[1.930,1.990]	37299 ± 633	10.46 ± 0.01	5.52 ± 0.24
$K_S^0 K^+ \pi^- \pi^-$	[1.950,1.985]	13475 ± 350	18.74 ± 0.03	10.00 ± 0.66
$\pi^+ \pi^- \pi^-$	[1.950,1.985]	34918 ± 688	50.32 ± 0.03	23.08 ± 1.07
$\pi^- \eta$	[1.930,2.000]	16951 ± 222	42.83 ± 0.04	23.10 ± 1.59
$\pi^- \pi^0 \eta$	[1.920,1.995]	27631 ± 785	14.69 ± 0.01	9.04 ± 0.55
$\pi^- \eta'(\pi^+\pi^-\eta)$	[1.940,2.000]	8675 ± 120	21.51 ± 0.04	8.98 ± 0.78
$\pi^- \eta'(\gamma\pi^+\pi^-)$	[1.945,1.980]	22720 ± 524	27.48 ± 0.03	13.49 ± 1.04
$K^- \pi^+ \pi^-$	[1.950,1.985]	15801 ± 463	44.82 ± 0.04	23.64 ± 1.75

the generic MC samples are summarized in Table I for each individual ST mode.

The signal $D_s^+ \to p\bar{n}$ and the isolated photon from the D_s^* decay are reconstructed from the remaining tracks and photons that are not used in the ST D_s^- reconstruction. Exactly one remaining charged track with opposite charge to the ST D_s^- meson and at least one remaining good photon are required. The charged track is identified as a proton by requiring $\mathcal{L}(p) \geq \mathcal{L}(K)$, $\mathcal{L}(p) \geq \mathcal{L}(\pi)$ and $\mathcal{L}(p) \geq 0.001$. The angle between this isolated photon and the nearest charged track is required to be larger than 10°.

To improve the resolution and the likelihood of associating the correct photon candidate from the D_s^* decay, we perform a kinematic fit with constraints on the masses of the ST D_s^-, signal D_s^+, intermediate state $D_s^{*\pm}$, and the initial four-momentum. The two hypotheses, i.e., $e^+e^- \to D_s^{*+}(\gamma + p\bar{n})D_s^-(\text{ST})$ or $e^+e^- \to D_s^+(p\bar{n})D_s^{*-}(\gamma + \text{ST})$, are tested, and the one with the smaller fit χ^2 is chosen. In the fit, the antineutron is treated as a missing particle with unknown mass, thus there are 7 constraints and 4 unknown parameters. The χ^2 of the kinematic fit is required to be less than 200. This requirement retains most of the signal events, but removes 50% of background. For an event with more than 1 remaining photon, we try all photon candidates in the kinematic fit, and the one with the smallest χ^2 is selected. The updated momenta after the kinematic fit are used in the subsequent analysis. The resulting mass of the missing particle M_{miss}, using all ST modes, is shown in Fig. 2. A prominent antineutron signal is visible.

The potential backgrounds are classified into (a) non-D_s^- background and (b) real-D_s^- background. The background (a) is dominated by continuum processes with proton and antineutron in the final state and can be estimated with the events in the M_{tag} sideband region (3.5–5.0σ away from the D_s peak). The corresponding M_{miss} distribution of

background (a) is shown as the shaded histogram in Fig. 2. No obvious peak is observed in the vicinity of the antineutron signal. Since $D_s^+ \to p\bar{n}$ is the only baryonic decay mode for the D_s^+ meson, no peaking background is expected for background (b). The properties of the backgrounds are validated by studying the generic MC samples.

The total DT signal yield is determined by performing an unbinned maximum likelihood fit to the M_{miss} distribution in Fig. 2, where the signal is described by an MC-simulated line shape convolved with a Gaussian function representing the resolution difference between data and MC simulation; the background is modeled by an ARGUS function [17]. The fit shown in Fig. 2 returns 193 ± 17 $D_s^+ \to p\bar{n}$ signal events. The DT efficiencies for the individual ST mode are estimated by performing the same procedure on the generic MC samples, and are
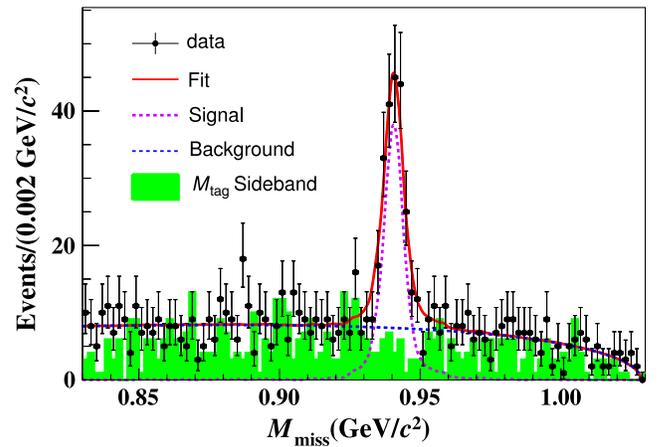

FIG. 2.   Fit to the M_{miss} distribution. The dots with error bars represent data, the (green) shaded histogram shows the events in the M_{tag} sideband region. The (red) solid line is the overall fit, the (violet) dotted line is the signal component, and the (blue) dashed line is the background component from the fit.

summarized in Table I. Based on Eq. (3), inserting all the numbers reported above and incorporating the world-average value for $\mathcal{B}(D_s^{*+} \to \gamma D_s^+)$ [14], we obtain $\mathcal{B}(D_s^+ \to p\bar{n}) = (1.21 \pm 0.10) \times 10^{-3}$, where the uncertainty is statistical only.

With a DT technique, the systematic uncertainties on detecting the ST D_s^- meson largely cancel. For the reconstruction of the isolated photon and the signal $D_s^+ \to p\bar{n}$, the following sources of systematic uncertainties are studied, resulting in a total systematic uncertainty of 4.4% when the individual contributions are summed in quadrature.

The efficiencies for proton tracking and PID are studied as function of $\cos\theta$ and momentum using the control sample $e^+e^- \to \pi^+\pi^- p\bar{p}$. The results are then weighted by the $\cos\theta$ and momentum distributions of the proton in the signal MC. The average efficiency difference between data and MC simulation combined for tracking and PID is 3.2%, which is taken as the systematic uncertainty.

We study the uncertainties associated with the photon detection and the kinematic fit simultaneously with a control sample of $D_s^+ \to K_S^0 K^+$ decays produced in the process $e^+e^- \to D_s^{*+}D_s^- \to D_s^+\gamma D_s^-$. The resultant difference on the efficiencies between data and MC simulation is 2.4%, which is assigned as the systematic uncertainty from this source.

The proton and antineutron may produce additional showers in the EMC that might then affect the efficiency of detecting $D_s^+ \to p\bar{n}$ decays. To estimate this effect, we examine the detection efficiencies determined with two different signal MC samples that are produced with and without the neutron interaction effect in the EMC, respectively. Conservatively, we assign half of the difference between the two efficiencies, 0.9%, as the uncertainty.

The uncertainty sources associated with the fit to the $M_{\rm miss}$ distribution include the background parameterization and the fit range. The corresponding uncertainties are estimated by performing fits with alternative background shape obtained with the events in the ST $M_{\rm tag}$ sideband region and various fit ranges. The resultant changes on the signal yields are regarded as the corresponding uncertainties. The sum of the three uncertainties above in quadrature is 0.7%, which is taken as the associated systematic uncertainty.

For the ST D_s^- yields, there is a contribution from the process $e^+e^- \to \gamma_{\rm ISR}D_s^+D_s^-$, which causes a tail falling into the $M_{\rm rec}$ windows. We estimate this background contributes to our ST yields by at most 0.3% based on the MC simulation. We take this upper limit as the systematic uncertainty from this source.

According to Eq. (3), the uncertainty related to the ST efficiency is expected to be canceled. However, due to the different multiplicities, the ST efficiencies estimated with the generic and the signal MC samples are expected to differ slightly. Thus, the uncertainty associated with the ST

efficiency is not canceled fully, which results in a so called "tag bias" uncertainty. We study the tracking/PID efficiencies in different multiplicities, and take the combined differences between data and MC simulation, 0.6%, as the corresponding uncertainty.

The uncertainties associated with the quoted BF of $D_s^{*+} \to \gamma D_s^+$ and the limited MC statistics are also considered, which lead to 0.8% and 1.1%, respectively.

In summary, using an e^+e^- collision data sample corresponding to 3.19 fb^{-1} collected at $\sqrt{s} = 4.178$ GeV with the BESIII detector, we report the observation of $D_s^+ \to p\bar{n}$ and measure the absolute BF to be $(1.21 \pm 0.10 \pm 0.05) \times 10^{-3}$, where the first uncertainty is statistical and second systematic. The decay $D_s^+ \to p\bar{n}$ is confirmed and the precision of the BF measurement is much better than that of the previous measurement [6]. The large BF for $D_s^+ \to p\bar{n}$ explicitly shows that the weak annihilation process featured as a short-distance dynamics is not the driving mechanism for this transition, while the hadronization process driven by nonperturbative dynamics determines the underlying physics. The measurement is important since similar annihilation effect is also present in other hadronic decays of charmed mesons. Relating this baryonic decay rate to the leptonic rate should provide important clues on how baryons are produced in hadronic interactions. The improved measurement also sets up the nonperturbative scale, allowing a better understanding of the transition mechanism. This high precision measurement can be taken as evidence for the role played by the hadronization process and is useful for improving existing and developing further models.

[1] S. S. Gershtein and M. Y. Khlopov, JETP Lett. **23**, 338 (1976).

[2] X. Y. Pham, Phys. Rev. Lett. **45**, 1663 (1980).

[3] I. Bediaga and E. Predazzi, Phys. Lett. B **275**, 161 (1992).

[4] C. H. Chen, H. Y. Cheng, and Y. K. Hsiao, Phys. Lett. B **663**, 326 (2008).

[5] I. I. Y. Bigi and N. G. Uraltsev, Phys. Lett. B **280**, 271 (1992).

[6] S. B. Athar *et al.* (CLEO Collaboration), Phys. Rev. Lett. **100**, 181802 (2008).

[7] Y. K. Hsiao and C. Q. Geng, Phys. Rev. D **91**, 077501 (2015).

[8] M. Ablikim *et al.* (BESIII Collaboration), Nucl. Instrum. Methods A **614**, 345 (2010).

[9] X. Wang *et al.*, J. Instrum. **11**, C08009 (2016).

[10] S. Agostinelli *et al.* (GEANT4 Collaboration), Nucl. Instrum. Methods A **506**, 250 (2003).

[11] R. G. Ping, Chin. Phys. C **38**, 083001 (2014).

[12] E. Richter-Was, Phys. Lett. B **303**, 163 (1993).

[13] D. J. Lange, Nucl. Instrum. Methods A **462**, 152 (2001); R. G. Ping, Chin. Phys. C **32**, 599 (2008).

[14] C. Patrignani *et al.* (Particle Data Group), Chin. Phys. C **40**, 100001 (2016).

[15] J. C. Chen, G. S. Huang, X. R. Qi, D. H. Zhang, and Y. S. Zhu, Phys. Rev. D **62**, 034003 (2000).

[16] X. Ma *et al.*, Chin. Phys. C **32**, 744 (2008); Y. H. Guan, X. R. Lu, Y. H. Zheng, and Y. F. Wang, Chin. Phys. C **38**, 016201 (2014).

[17] H. Albrecht *et al.* (ARGUS Collaboration), Phys. Lett. B **241**, 278 (1990).